Sustainable Zero Liquid Discharge of Concentrated Brine by Janus Wood Evaporator

Xi Chen
Department of Civil and Environmental Engineering, Princeton University https://orcid.org/0000-0003-2360-2672
Shuaiming He
University of Maryland, College Park
Mark Falinski
Princeton University
Yuxi Wang
Princeton University https://orcid.org/0000-0001-9597-469X
Tian Li
University of Maryland, College Park
Sunxiang Zheng
Princeton University
Dongya Sun
Princeton University
Jiaqi Dai
University of Maryland College Park
Yanhong Bian
Princeton University
Xiaobo Zhu
Princeton University
Jinyue Jiang
Princeton University
Liangbing Hu
University of Maryland, College Park https://orcid.org/0000-0002-9456-9315
Zhiyong Ren (zjren@princeton.edu)
Princeton University https://orcid.org/0000-0001-7606-0331

Article

Keywords: Sustainable, Water-energy nexus, Solar distillation, Janus wood evaporator, Life cycle assessment

Posted Date: February 24th, 2021

DOI: https://doi.org/10.21203/rs.3.rs-253797/v1

Sustainable Zero Liquid Discharge of Concentrated Brine by Janus Wood Evaporator

Xi Chen[1], Shuaiming He[2], Mark M. Falinski[1], Yuxi Wang[1,3], Tian Li[2], Sunxiang Zheng[1], Dongya Sun[1], Jiaqi Dai[2], Yanhong Bian[1], Xiaobo Zhu[1], Jinyue Jiang [1], Liangbing Hu[2]*, and Zhiyong Jason Ren[1]*

[1] Department of Civil and Environmental Engineering and Andlinger Center for Energy and the Environment, Princeton University, Princeton, NJ 08544, United States

[2] Department of Materials Science and Engineering, University of Maryland, College Park, MD 20742, United States

[3] The Earth Institute and School of International and Public Affairs, Columbia University, New York, NY 10027, United States

*Corresponding authors:
Liangbing Hu: binghu@umd.edu;
Zhiyong Jason Ren: zjren@princeton.edu

Key words: Sustainable, Water-energy nexus, Solar distillation, Janus wood evaporator, Life cycle assessment

Abstract

Solar-driven distillation is a promising technology for energy-efficient freshwater generation, but salt accumulation on solar absorbers and system longevity are major challenges that hinder its widespread application. In this study, we present a novel Janus wood evaporator that overcame these challenges and achieved record-high evaporation efficiencies in high-salinity brine, one of the most difficult water sources to treat using desalination. The Janus wood evaporator had an asymmetric surface wettability, where the top layer acted as a hydrophobic solar absorber with enhanced thermal insulation, while the bottom hydrophilic wood layer allowed for rapid water replenishment. An evaporation efficiency of 82.0% was achieved for 20% NaCl solution, and superior salt-resistance was observed during a 10-cycle longevity test. To ensure the environmental sustainability of the new Janus wood evaporator, a life cycle assessment (LCA) was conducted to compare this Janus wood evaporator to emerging Janus evaporators. Results showed that Janus wood evaporators could emit up to two orders of magnitude less CO_2 equivalents than an aerogel Janus evaporator (AJE) and up to 80% fewer emissions than an electrospun Janus mat (EJM), indicating a functional and more sustainable opportunity for off-grid industrial applications and humanitarian efforts.

Introduction

The growing threats of global freshwater scarcity and climate change are driving an increased reliance on unconventional water sources such as seawater or brackish groundwater.[1,2,3] As a result, water desalination capacity has more than tripled over the past 20 years.[4] However, traditional water desalination has a high energy demand and high cost, and brine disposal remains a major application barrier.[5,6] With the existing benchmark process, reverse osmosis (RO), reaching its energy efficiency limit (~50%),[7] integration with renewable energy and low-energy processes becomes essential to make desalination affordable and sustainable. In this context, novel solar distillation processes carry strong promise, as they take advantage of abundant, efficient, and low-cost solar energy and have the potential to reach the goal of zero liquid discharge (ZLD).[8,9,10]

Solar-driven water distillation is a facile process that doesn't require electricity infrastructure and can be modularized for easy deployment.[11,12] Unlike pressure-driven processes, solar evaporators can effectively treat high-salinity water without a significant energy consumption.[13] Modern solar evaporators have increased evaporation efficiency compared to traditional processes by enhancing light absorption and minimizing heat losses[14, 15 ,16,17,18], but salt accumulation and system longevity are still major challenges that hinder widespread adoption.[19,20,21] During solar-driven distillation, the salt concentration continuously increases on the photothermal material surface leading to crystallization,[22] which can result in severe performance drop due

to the physical blocking of solar absorption sites, which acts to decrease steam generation.[23] Attempts have been made to solve such problem by using nanomaterial-based Janus thin-film evaporators with asymmetric surface wettability, and results showed that desalination performance remained stable without severe salt accumulation under low-salinity conditions (~3.5%wt). [24,25] However, there is a great need for systems that can handle high salinity brines that are generated at desalination facilities (20-25%wt). These waste streams are considered the “Achilles’ heel of desalination”, as they are costly to manage and dispose of at any scale.[26,27] Furthermore, these Janus thin-film evaporators, with a thickness of <1 mm, had inferior thermal insulation and evaporation efficiency. To achieve better performance, thicker Janus evaporators would need to be utilized. However, this would likely increase cost and fabrication complexity, as well as the environmental impact of the whole system.

While a high level of performance is essential, there is also concern about the environmental impact of the evaporator material. The majority of current solar evaporators are made of petroleum-based products or nanomaterials, which have a considerably high environmental impact and carry a high cost that prevents their use in large-scale applications. Therefore, more sustainable materials like natural wood can instead serve as an alternative evaporator material for more sustainable solar steam generation. However, natural wood evaporators suffer from severe salt-accumulation and a corresponding performance decay,[28] and the only way to achieve salt-rejection was based on the alternative salt pathways through large holes that

leads to unsatisfactory heat localization and low evaporation efficiency (57~75%).[13,28]

In this study, we present a novel Janus wood evaporator with asymmetric wettability for solar distillation toward clean water that guaranteed great salt-resistance, thermal insulation, and evaporation efficiency (**Fig. 1a**). Among all reported Janus evaporators, the newly engineered Janus wood evaporator achieved the highest evaporation efficiency and maintained stable performance in the highest salinity (20%wt) brines, while proving to be the most sustainable evaporative system (**Fig. 1b**). Additionally, for the first time, a life cycle assessment (LCA) for solar distillation systems was developed and compared the Janus wood with other nanomaterial-based Janus evaporators and high-pressure desalination systems to evaluate each systems' relative embodied carbon during the extraction, manufacturing, and use phases (**Fig. 1c**). Taking into consideration the facile fabrication, wide availability of wood materials, low cost, stable performance, and relatively low global warming potential, Janus wood evaporators have the potential to be an ideal solution for sustainable water desalination and ZLD.

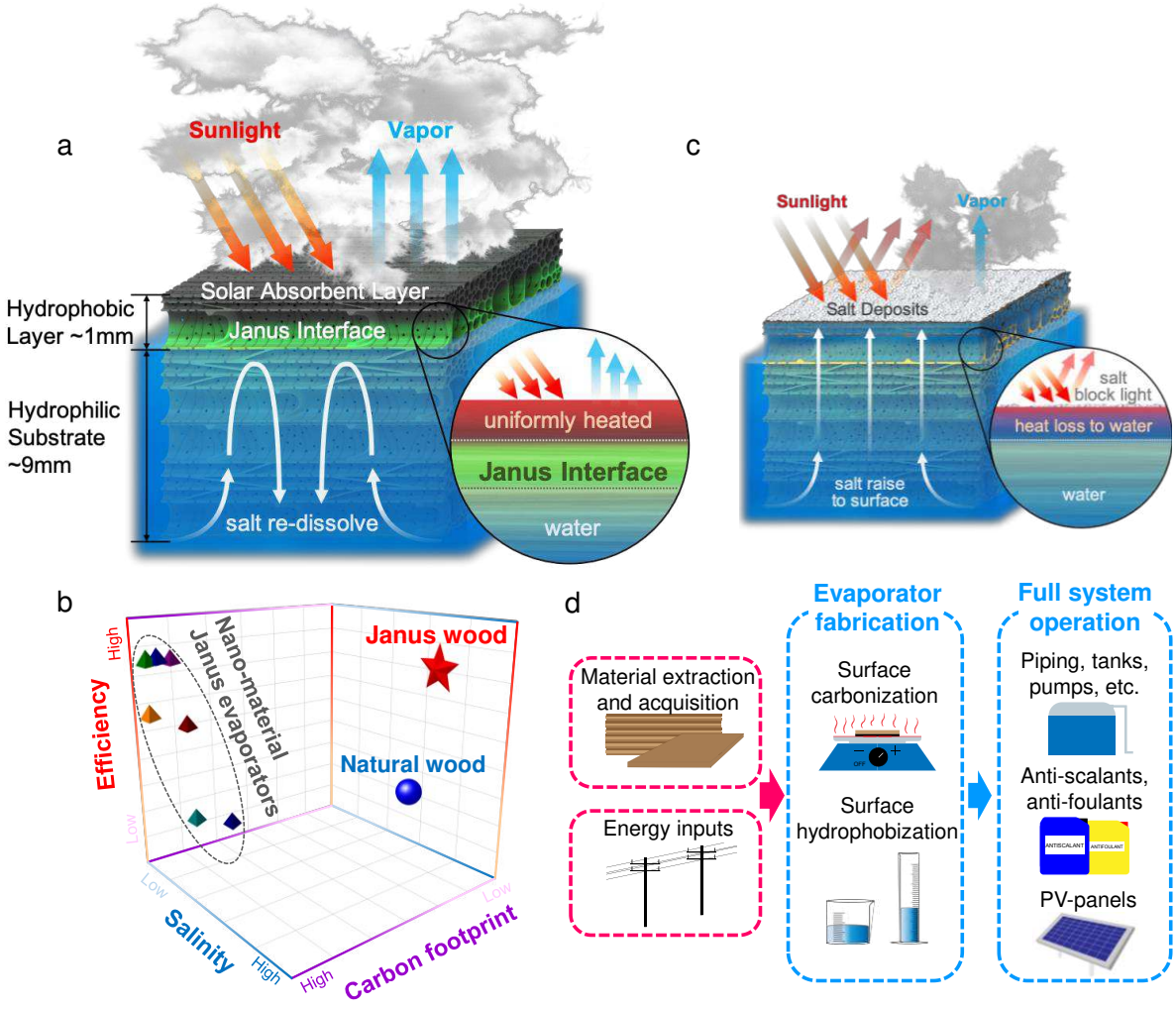

Figure 1. **Janus wood as a salt-resistant and sustainable evaporator. a**, Schematic of the Janus wood evaporator for solar distillation, where the Janus interface enhanced thermal insulation and improved performance. **b**, Performance comparison of Janus wood evaporator, natural wood evaporator and nanomaterial-based Janus thin-film evaporator. **c**, Salt accumulation caused severe performance decay in a natural wood evaporator. **d**, Scope of the life cycle assessment for the Janus wood evaporator ZLD system.

Principle of the Janus wood evaporator. Water and salt crystals reflect solar irradiation, which lead to reduced efficiency, and as a result, the solar absorber surface needs to be kept dry and clean to maintain high solar absorption. However, for traditional solar evaporators with uniform hydrophilic structures, saline water is directly lifted onto the evaporator surface, where water quickly evaporates, leaving behind salt

deposits, which could hinder solar-absorption and block evaporation (**Fig. 1c**). To decouple the evaporative process from the solar absorption surface and prevent salt accumulation, the Janus wood evaporator has a thin hydrophobic solar absorber surface layer with a thick hydrophilic wood substrate bottom layer (**Fig. 1a**). Saline water is lifted upward by capillary force through the hydrophilic mesoporous wood structure, stopping at the hydrophilic-hydrophobic Janus interface. In doing so, the water-air interface is relocated inside the evaporator instead of on the top layer. Despite the increase in the local salt concentration at this water-air interface during water evaporation, the salt ions could freely diffuse back to the water reservoir, rather than form solid crystals. Meanwhile, the hydrophobic top layer improved heat localization and reduced heat loss, allowing the surface temperature of the Janus wood evaporator to be higher than that of a uniform natural wood evaporator (Supplementary **Fig. S1, S2**). As a result, a Janus wood evaporator has the potential for higher-efficiency solar desalination/ZLD with improved salt-resistance over previous, more uniform evaporators.

Janus wood evaporator design. Two common tree species, Basswood and Balsawood, were tested as potential Janus wood evaporators. For each sample, natural wood was cut longitudinally and radially and then underwent surface carbonization (Supplementary **Fig. S3, S4, S5**). Then, the surface temperature and solar distillation performance was tested under the same solar conditions (Supplementary **Fig. S6, S7**). Basswood with parallel cutting showed the best overall

performance (details in Supplementary Note 1) and was therefore used in the subsequent studies.

Fig. 2 shows the morphology and physical characterizations of the Janus wood evaporator. The fabricated Janus wood underwent surface carbonization to increase photothermal conversion and was then functionalized by perfluorodecyltriethoxysilane (FAS) to improve hydrophobicity. The top surface of the Janus wood rejected liquid water penetration and had a large contact angle of 141° (**Fig. 2b**), while the untreated surface control sample remained highly hydrophilic with a contact angle of 32° (Supplementary **Fig. S8**). The contact angle of the FAS-treated Janus wood surface was among the highest relative to more expensive nanoparticle hydrophobic layers commonly found in Janus film evaporators, including carbon black nanoparticles coated with polymethylmethacrylate (PMMA), gold nanorods (AuNR), and Ti_3C_2 nanosheets. [24,25,29] The superior hydrophobicity of the Janus wood surface was attributed to the FAS treatment, which has a very low surface energy of 13.1 mN m^{-1} and is highly effective in modifying the abundant -OH groups on the cellulose in wood (Supplementary **Fig. S9**). In contrast to the top surface, the bottom surface of the Janus wood remained highly hydrophilic (contact angle of 28°) and was quickly wetted by water (**Fig. 2c**). The contrasting chemical properties on each side of the Janus wood guaranteed fast saline water transport from the bottom via capillary force, while inhibiting salt accumulation on the top solar absorber layer.

In addition, the unique hierarchical mesoporous structure of Janus wood enabled fast mass transport and excellent heat localization and insulation. Scanning electron microscopy (SEM) images depict an abundance of channels aligned horizontally in the Janus wood (**Fig. 2d**). These channels are tree vessels (~50 μm in diameter) and tracheid (~10 μm in diameter) that form along the growth direction,[30] which were well-preserved from the wood block after carbonization and hydrophobization. These channels are aligned parallelly (**Fig. 2e**) and interconnected via small pores called pits (1~2 μm in diameter), which are distributed along the vessel walls (**Fig. 2f, 2g**). The channels and pits form a 3-dimensional mass transfer network inside the wood. The big channels facilitate ion diffusion in the horizontal direction and help equalize saline water concentration to prevent local salinity build-up and crystallization. Meanwhile, the small pits on vessel walls allow fast water convection and ion diffusion in the vertical direction. Moreover, the anisotropic structure of Janus wood allows for a very low thermal conductivity of ~0.11 $Wm^{-1}K^{-1}$, which increases thermal insulation and heat localization in the vertical direction and enables higher-efficiency solar-driven evaporation. [31]

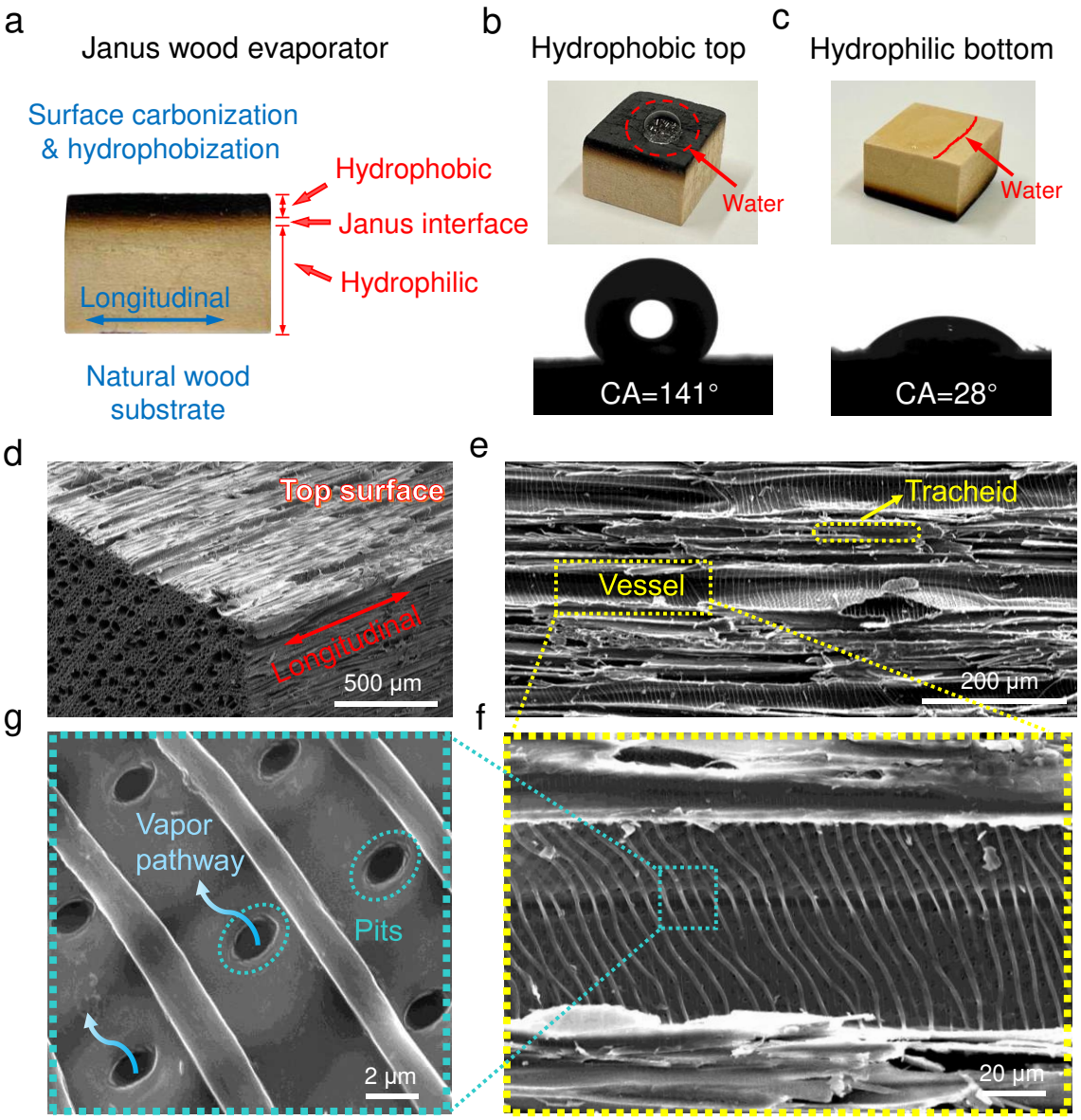

Figure 2. Characterization showing the asymmetric wettability and the hierarchical porous structure of the Janus wood evaporator. a, The digital image of Janus wood evaporator. **b**, The top surface was modified into hydrophobic with a large contact angle (CA) and rejected water penetration. **c**, The bottom layer maintained the hydrophilic nature of wood and was quickly wetted by water drops. **d**, SEM image showing the hierarchical structure of Janus wood. **e**, Magnified SEM image showing aligned vessels and tracheid on the top surface, **f**, Magnified SEM image showing vessel wall structure. **g**, magnified SEM images showing the abundantly distributed pits on the vessel wall.

Record-high performance with concentrated brine. The photothermal conversion performance was tested using an optical solar incidence of 3 suns, and the surface

temperature difference between the Janus wood evaporator and a natural wood evaporator without FAS treatment was compared. Results showed that the surface temperature of the natural wood control increased from 22.4 °C to 47.2 °C after 1 min. Meanwhile, the surface temperature of Janus wood increased from 22.2 °C to 56.1 °C within 1 min (**Fig. 3a**). The stable surface temperature of Janus wood evaporator under 3 suns could reach 64.7 °C after 15 min, while the bulk brine temperature remained below 29 °C (**Fig. 3b**). In contrast, the natural wood evaporator reached a lower surface temperature of 57.5 °C after 15 min, while the bulk brine reached a higher temperature (30.5 °C).

COMSOL was used to simulate the temperature distribution and heat transfer in the Janus/natural wood solar distillation systems. The hydrophobic top layer filled with air/vapor has a low thermal conductivity of ~0.1 $Wm^{-1}K^{-1}$, which enhanced heat insulation and localization in the Janus wood evaporator (**Fig. 3c**), and supported a large temperature gradient of 35.7°C. In contrast, the top layer of natural wood evaporator was filled with water with inferior heat insulation (Supplementary **Fig. S1b**). **Fig. 3d** shows the high temperature gradient between the top and bottom layers of the Janus wood evaporator under varying intensity of solar incidence. Under 1 sun, the surface temperature reached 44.7 °C, which was among the highest from published solar evaporator studies. From 0.5 sun to 3 suns, the top surface temperature of the Janus wood substantially increased from 34.3 to 64.7 °C, while the bottom brine temperature remained relatively stable, only increasing from 24.6 °C to 29.0 °C under

the same conditions. These results confirm the relatively high thermal insulation properties of the Janus wood evaporator.

Fig. 3e depicts the evaporation rate (E.R.) and evaporation efficiency (E.E.) of the Janus wood at different feed solution salinities (0%, 5%, 10%, and 20%) under 1 sun illumination. The E.R. slightly decreased from 1.35 $kg \cdot m^{-2} \cdot h^{-1}$ to 1.20 $kg \cdot m^{-2} \cdot h^{-1}$ as salinity increased from 0% to 20%, while the E.E. gradually dropped from 92.3% to 82.0% (**Fig. 3e**). Such drops were expected as higher salinity resulted in a lower vapor pressure, which can hinder evaporation.[32] Of note, the E.E. of 87.6% for 5% NaCl solution was the highest of all published Janus thin-film evaporators (51%~83.5%), even though most of them operated at a lower salinity of ~3.5% (Supplementary **Table S1**). Even at a high salinity of 20%, which has rarely been investigated, Janus wood had a very high E.E. of 82.0%. This efficiency was also much higher than in other studies used wood-based evaporators to distill feed solutions with lower salt concentrations (15% NaCl; E.E. of 57%~75%).[13,28] Under larger solar fluxes, Janus wood achieved even higher E.R. of 2.39 $kg \cdot m^{-2} \cdot h^{-1}$ for 2 suns and 3.69 $kg \cdot m^{-2} \cdot h^{-1}$ for 3 suns, with a corresponding E.E. of 83.6% and 86.8%, respectively (**Fig. 3f**). Even for the lower optical concentration of 0.5 sun, which could be representative of the natural environment, the E.R. reached 0.59 $kg \cdot m^{-2} \cdot h^{-1}$ with a good E.E. of 76.5%, indicating the viability of the Janus wood evaporator in real-world applications.

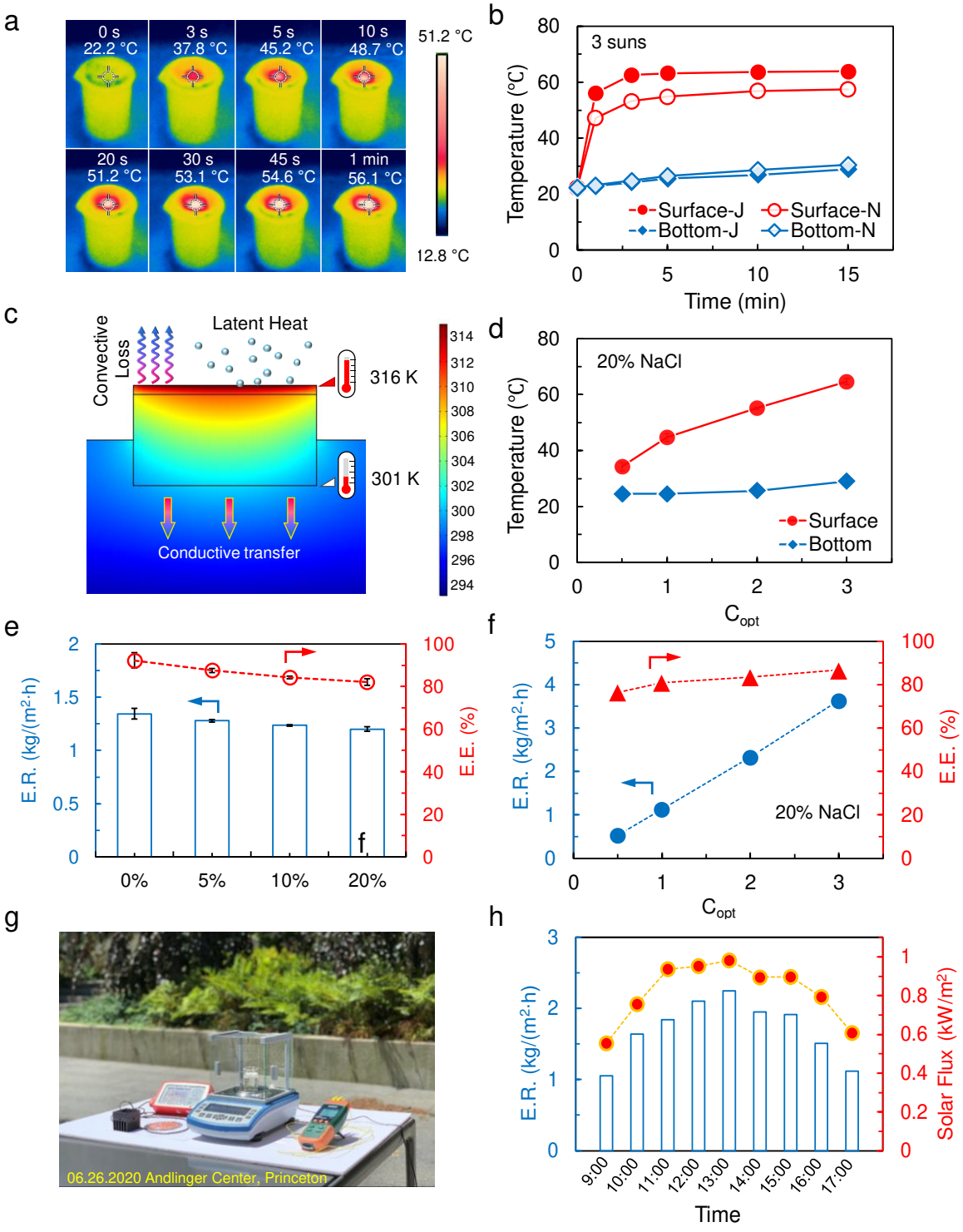

Figure 3. High solar distillation performance of Janus wood evaporator in lab conditions and field tests. a, IR images of the solar distillation module under 3 suns at increasing times up to 60s. **b**, Time-dependent surface temperature changes of the Janus wood (J) and natural wood control (N) under 3 suns illumination. **c**, Cross-sectional temperature profile of the Janus wood evaporator and the bulk brine under 1 sun incident, modelled with COMSOL, indicating the hydrophobic top layer improved heat insulation and localization. **d**, Surface temperature changes of Janus wood under

different optical concentrations. **e**, The evaporation rate (E.R.) and evaporation efficiency (E.E.) of Janus wood under different salinities. **f**, The E.R. and E.E. of Janus wood under different solar incident concentrations. **g**, Digital image of the solar distillation module setup. **h**, The hourly-average E.R. corresponding to the hourly-average natural solar flux.

We also conducted field tests under natural conditions with varying solar flux and wind (**Fig. 3g**). The experiments were conducted from 9:00 to 17:00 in June in Princeton, New Jersey, using a 20% NaCl solution. The relative humidity was 50~60% and the ambient temperature was 26~35 °C. **Fig. 3h** shows a strong correlation between the hourly average E.R. and the solar flux. At the maximum solar flux of 0.98 kW/m^2, the highest E.R. was 2.25 kg·m^{-2}·h^{-1}. The E.E. ranged from 131% to 167% during the field test, which indicates that natural wind considerably accelerated evaporation on top of the solar-thermal driving force. The field tests proved that the Janus wood evaporator was able to maintain its desalination performance under naturally varying solar incidence, which indicates its promising potential in real-world applications.

System longevity and persistent salt-resistance. System longevity was tested by operating the Janus wood evaporator alongside the natural wood evaporator for ten consecutive cycles. For each solar distillation cycle, the evaporator operated continuously for 8 hours under 1 sun, followed by 16 hours in the dark to simulate natural daylight cycling. **Fig. 4a** shows the surface of the natural wood control over the course of the ten cycles. At the beginning of the test, the surface of the natural wood was easily wetted, and salt started to accumulate after the 1st cycle, almost covering the entire surface of the natural wood. By the end of 10th cycle, a thick salt shell formed

across the whole evaporator (**Fig. 4a**). In contrast, the surface of the Janus wood evaporator was dry and clean at the beginning. After the 1st cycle, no salt accumulation was observed on the surface (**Fig. 4b**), and after the 10th cycle, the surface of Janus wood remained clean and dry, with only a small number of salt crystals on the evaporator edge. This is likely attributed to the leakage of saline water through the gap between the evaporator and foam holder, not through the evaporator itself. The images clearly show improved salt rejection by the Janus wood evaporator as a result of its hydrophobicity.

Fig. 4c compares the E.R. of two wood evaporators during the 1st cycle. It can be seen that the E.R. of the natural wood evaporator quickly increased to 1.08 $kg \cdot m^{-2} \cdot h^{-1}$ within 60 min, but soon started to decay and hit a low level of 0.40 $kg \cdot m^{-2} \cdot h^{-1}$. The SEM image taken at 1 h clearly showed that salt crystallization blocked a significant area on the natural wood evaporator (**Fig. 4d**). Therefore, the 63% decrease in E.R. was believed to be primarily attributed to salt accumulation on the surface, which scattered solar incident and hindered vapor transport. In comparison, the E.R. of the Janus wood evaporator quickly increased to >1.20 $kg \cdot m^{-2} \cdot h^{-1}$ after 120 min and then remained at the same level without decay for the whole 8-hour cycle (**Fig. 4c**). As expected, the SEM investigation of Janus wood showed a very clean surface without salt accumulation, where the channeled surface structure of the Janus wood evaporator could be clearly observed (**Fig. 4e**). By the end of the cycle, the E.R. for Janus wood was nearly 3 times larger than that of the natural wood evaporator.

Similar differences were observed in the 10-day, 10-cycle longevity test. During this period, the surface temperature of the Janus wood remained at around 44 °C, likely as a result of the clean and dry surface, which enabled high-efficiency solar-heat conversion (**Fig. 4f**). However, the surface temperature of the natural wood decreased from 41.7 °C at the beginning to 35.5 °C at the end of 1st cycle, which then further decreased to 33.0 °C by the end of the 10th cycle.

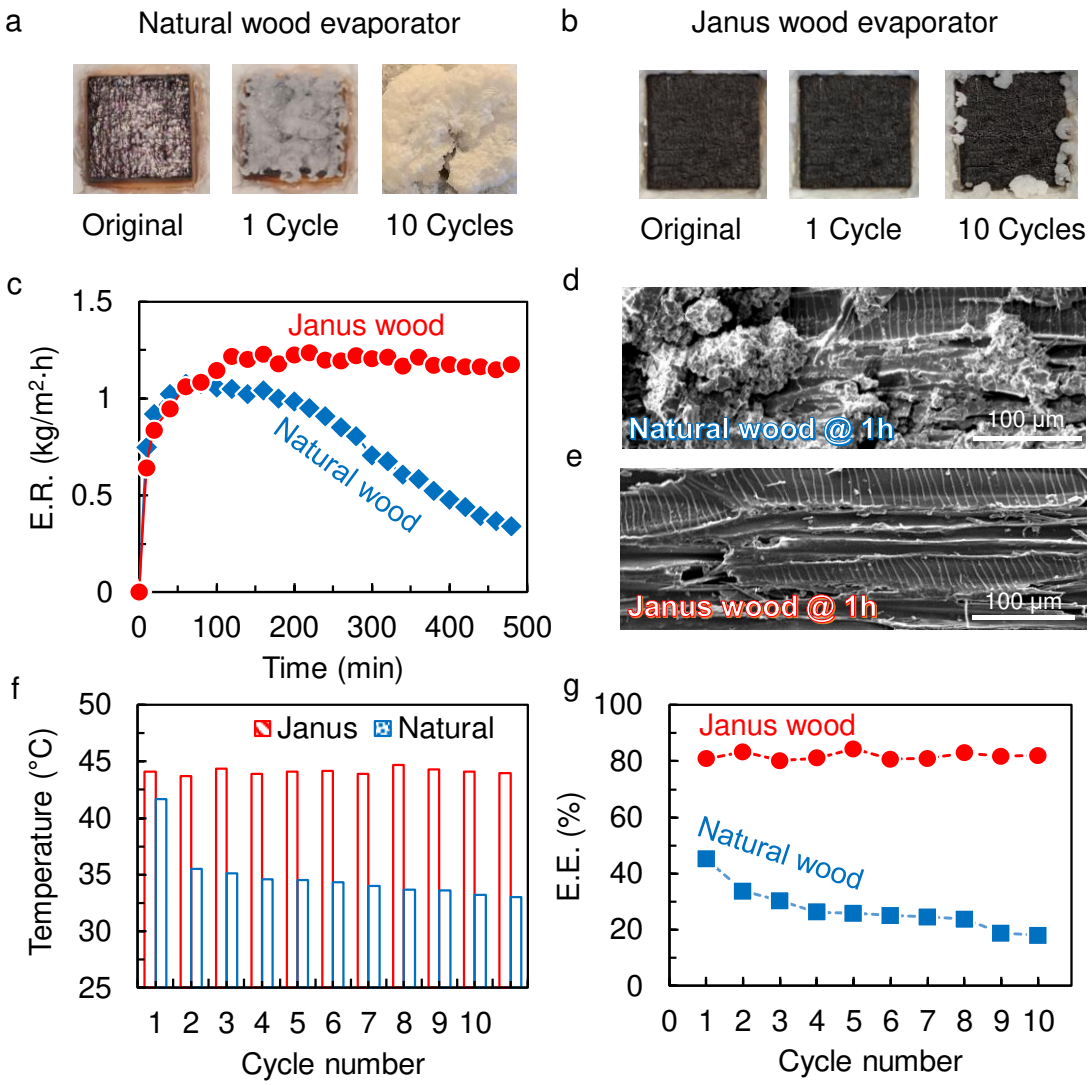

Figure 4. Longevity tests of the Janus wood and natural wood. a, Digital images of the natural wood evaporator before cycling experiments, after the 1st cycle, and after the 10th cycle. **b,** Digital images of the Janus wood evaporator before cycling experiments, after the 1st cycle, and after the 10th cycle. **c,** The evaporation rate (E.R.) of the wood evaporators during the 1st cycle. **d**, SEM image of the top surface of the

natural wood evaporator after operating for 1 hour in the 1st cycle. **e**, SEM image of the top surface of the Janus wood after operating for 1 hour in the 1st cycle. **f**, The surface temperature of the Janus wood v.s. natural wood in each of the 10 cycles. **g,** The evaporation efficiency (E.E.) of the Janus wood and natural wood in each of the 10 cycles.

The E.E. of the Janus wood evaporator remained very stable at > 80% during the longevity test, while the E.E. of the natural wood evaporator decreased from 45.2% during the 1st cycle to 18.0% during the 10th cycle, indicating a severe performance decline, due to salt accumulation (Fig. 4g). This downward trend kept occurring despite the stabilization of surface temperatures after the 3rd cycle (Fig. 4f). This is likely due to the continuous salt accumulation that blocked the vapor escape pathway and raised the humidity at the surface, hindering evaporation. As a result, the E.E. of the Janus wood was 4.6 times larger than that of the natural wood evaporator at the end of the 10-day test. This proves that Janus wood evaporator has much better longevity and stability than a natural wood evaporator, and therefore holds a great promise toward practical solar distillation.

Life Cycle Assessment of the solar distillation systems. Few studies exist exploring the global warming potential (GWP) of ZLD technologies, and to our best knowledge no study has evaluated the GWP of Janus evaporators or other passive desalination systems. Therefore, to assess the environmental impacts of the Janus wood evaporator against comparable technologies, we conducted a preliminary life cycle assessment (LCA), based on ISO Standard 14040,[33] defaulting to lab- and pilot-scale data, except in the case of lab processes that are easily scaled-up to an industrial

equivalent. The detailed background was stated in Supplementary Note 2. The Janus wood evaporators from this study were compared to three other systems modeled in this paper: an aerogel Janus evaporator (AJE) operating with a solution of 12% NaCl,[34] an electrospun Janus mat (EJM) operating with a solution of 20% NaCl,[24] and a simplified RO system powered by either photovoltaics (PV) or on-grid (OG) electricity.[35] As the systems evaluated in this study do not exist in the ecoinvent v3.5 database, each system was built and compared side-by-side, based on industry and literature data. A majority of the CO_2 equivalent emissions (CO_{2e}) from each Janus evaporator system was a result of the evaporator production, since the environmental impacts of the tanks, photovoltaic panel, and pumps could be spread out over a 20-year period (Supplementary **Fig. S12**). A majority of the emissions from the systems featuring RO are a result of the high energy requirements in pump operation that either require energy from the grid, or very large photovoltaic panels (Supplementary **Fig. S13**).

Fig. 5 shows the result of the IPCC 2013 20a method for each system, based on the number of uses of each evaporator before replacement. Under ideal circumstances, where a single Janus wood evaporator could be used for the entire 20-year period (7300 uses), that system resulted in the lowest GWP per functional unit among all of the alternatives (**Fig. 5a**). Janus wood outperformed the other Janus evaporators, emitting 2 orders of magnitude less CO_{2e} than the AJE, and less than 20% of the CO_{2e} emissions of the EJM. However, with a shorter lifetime of each Janus wood evaporator,

the GWP of the system greatly increases. Even though a Janus wood evaporator used less than 100 times is more sustainable than the OG-RO system, one that cannot be used more than 250 times is less sustainable than a PV-RO system with a lifetime of 20 years (**Fig. 5a**). However, the OG-RO and PV-RO systems likely undercount the real emissions due to its oversimplicity, and the GWP related to backwashing or membrane and PV-panel replacements were not considered. Therefore, it is likely that the required lifetime of a Janus wood evaporator would actually be significantly less. More discussion of comparing the Janus wood evaporator with RO-based precipitation processes could be found in Supplementary Note 4.

This result is promising for Janus wood as a more environmentally-friendly option for passive ZLD systems. While a significant majority of the environmental impact of the Janus wood evaporator system came from the evaporator itself, this process has not been optimized, which means that emissions can be further lowered in the future. For example, based upon a preliminary analysis of the GWP of each input in the Janus wood evaporator (**Figure 5b**), the ethanol used during hydrophobization results in roughly 60% of the embodied CO_{2e} of the production of each evaporator, while the hydrophobic FAS (as modeled in this process) accounted for about 30% of the GWP of each evaporator. Focusing further research efforts toward the application of hydrophobic materials to carbonized wood would yield an even more environmentally-friendly zero liquid discharge system.

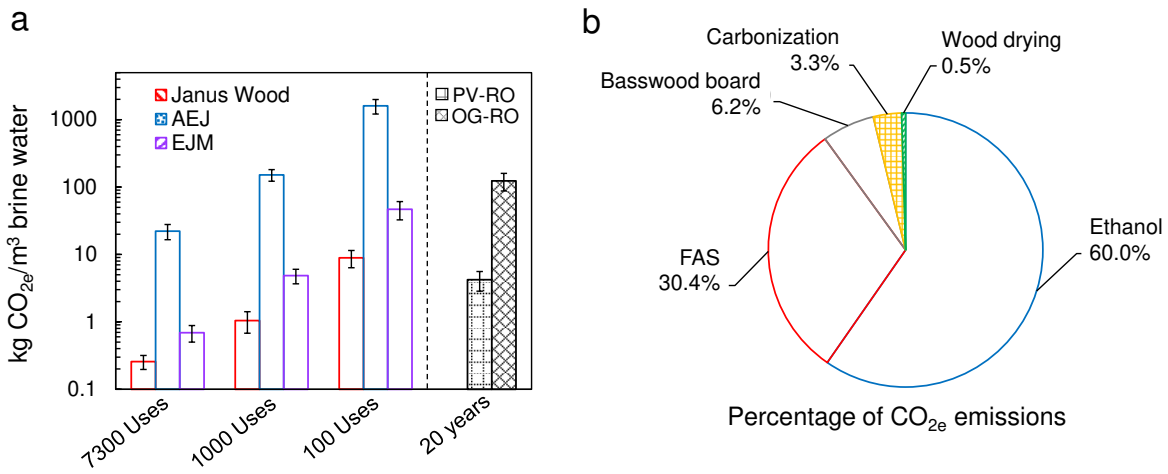

Figure 5. Preliminary LCA of the Janus wood evaporator and three other systems. a, The global warming potential of Janus wood evaporator, aerogel Janus evaporator (AEJ), and electrospun Janus mat (EJM), as it relates to the lifetime of each evaporator, as well as the global warming potential of photovoltaic (PV) and on-grid (OG) electricity-powered reverse osmosis (RO) systems. **b,** The relative CO_{2e} emissions of each process or material involved in the production of Janus wood evaporators.

Conclusion

In summary, a new Janus wood evaporator with asymmetric wettability for highly efficient and stable ZLD of concentrated brine was engineered in a sustainable manner for the first time. With the enhanced heat localization, better heat insulation, and higher surface temperature, the Janus wood evaporator achieved an impressive E.E. of 82.0% with 20% NaCl under 1 sun, which was appears to be the highest among the reported Janus evaporators operating under similar conditions. Moreover, the high salt-resistance led to very stable performance during long-term operation with an average evaporation efficiency of >80%, which was 4.6 times higher than the declining performance of a natural wood evaporator. The LCA demonstrated much lower CO_{2e} emissions in the Janus wood evaporator solar ZLD system versus other nano-material

based Janus evaporators. Further improvements and more sustainable systems could also be a result of greener materials and fabrication processes, including choosing other materials like bamboo with a lower GWP, improving heating and carbonization techniques, optimizing the thicknesses of both hydrophobic layer and bottom substrates, or exploring more environmentally-friendly hydrophobic chemicals. The Janus wood evaporator proposed in this study has a great potential to solve water-based problems in a practical, sustainable, and energy-efficient way.

Methods

Janus wood preparation. The most suitable base wood substrate was selected from two common tree species, Basswood and Balsawood, each with two cutting directions, parallel and vertical to the growth direction (Supplementary **Fig. S3**). After comparative testing, the basswood cut parallelly to the growth direction demonstrated the best potential and therefore was picked for preparing the Janus wood evaporator. A 1.5×1.5×1 cm wood block was tightly pressed on a 500°C hot plate for 45 s to create a carbonized solar-thermal layer. This layer was then polished with 2000 grit sandpaper and blown with compressed air to achieve a smooth and clean surface.[13] The carbonized layer was about 1 mm in depth and had a black appearance. The carbonized solar absorber layer was then hydrophobized using a FAS solution, which contained (weight%): 2% FAS (perfluorodecyltriethoxysilane, $C_{16}H_{19}F_{17}O_3Si$; Sigma-Aldrich), 3% ultrapure water, and 95% ethanol.[31] The pH of the solution was adjusted to 5.0 using acetic acid. This FAS solution was magnetically stirred for 24 h to ensure

complete hydrolysis and was evenly sprayed onto the carbonized side of the wood block. After the carbonized layer was completely covered by the FAS solution, the wood block was heated in a vacuum oven at 120 °C for 1 h at 80 kPa. The optical property of the carbonized solar absorber surface kept unchanged after the hydrophobization treatment (Supplementary **Fig. S15**). The final hydrophobic layer of the Janus wood was ~1 mm thick (Supplementary **Fig. S16**), consistent with the depth of the carbonized layer, and had a FAS loading of 8.9 ±0.7 mg/cm^2.

Material characterization. The contact angle was tested using a tensiometer (ramé-hart, Model 250) following a standard protocol. The morphology of wood evaporator samples was analyzed using scanning electron microscopy (FEI XL30 FEG-SEM). Thermography images were obtained from an infrared camera (FLIR, E5-XT). An ultraviolet-visible-near-infrared spectrophotometer (UV-vis, Lambda 35) equipped with an integrating sphere was used to detect the reflectance (R) and transmission spectra (T) of the solar absorber layer of the wood samples within 200–2500 nm, and the absorption (A) was calculated by: A=1-R-T.[13]

Solar distillation. The natural and Janus wood evaporators, with the carbonized sides facing up and away from the salt solution, were placed in a synthetic saline water reservoir and exposed to simulated sunlight generated by a solar simulator with 300 W Xe-arc lamps (Newport). Different concentrations NaCl solution (0-20%wt) were used in a suite of experiments with details explained in the results. The open area of

the saline solution surface around the wood evaporator was covered by polyethylene foam to prevent direct evaporation from the reservoir. The whole system including wood evaporator, sealing foam, saline water, and the container, was placed on an electronic scale (VWR, B2) with automated weight recording on a computer. The illumination intensity on the wood surface was tested by an optical power meter (THORLABS).[36] A thermocouple (Siemens) was used to measure the temperature change of the wood surface and the bulk saline solution during the experiments. The evaporation efficiency of the system was calculated using Equation (1):

$$\eta = \dot{m} \cdot h_{vap}/(C_{opt} \cdot P_0) \quad \text{(Equation 1)}$$

Where $\dot{m}$ is the evaporation rate under illumination subtracted the evaporation rate under dark condition; h_{vap} is the total enthalpy associated with water evaporation, which includes the sensible heat and the enthalpy of phase change; C_{opt} is the solar incident concentration; and P_0 is the nominal solar irradiation, 1 kW·m^{-2}. The experiments were performed at room temperature (~23°C) with a relative humidity of ~50%. Field tests were performed at Princeton, New Jersey, United States, with a 20% NaCl solution. The solar flux was measured every 10 min and was averaged hourly. The relative humidity during the field test was 50~60% and the ambient temperature was 26~35 °C.

Modeling. COMSOL Multiphysics software was used to evaluate the temperature distribution across the wood evaporators and the feed water reservoir. Geometry of the wood evaporator was set based on the experimental measurements. Taking

convective heat transfer to the ambient air and the internal convective/conductive heat transfer between the wood evaporator and feed water into consideration, the heat transfer in the semi-finite system could be expressed by Equation (2):

$$\mathrm{Q_{In}} = \rho C_p \frac{\partial T(x,t)}{\partial t} + \rho C_p \boldsymbol{u} \cdot \nabla T(x,t) + \nabla[\mathrm{k}\nabla T(x,t)] \quad \text{(Equation 2)}$$

where Q is the irradiative heat flux input; ρ, C_p, and k are the density, heat capacity and thermal conductivity of the medium (i.e., wood and water); $T(x,t)$ represent the local temperature at space vector x and time t; $\boldsymbol{u}$ is the velocity field in the system, which was set to zero for simplification. An external irradiation source that provides constant heat flux of 1000 W/m^2 was set on top of the wood evaporator. The ambient air temperature was set to be 293 K. The relevant parameter of water was loaded from material library built in COMSOL Multiphysics 5.5.

To simulate the latent heat for evaporation, we added a constant outward heat flux $\mathrm{Q_{Evap}}$ based on the experimentally acquired mass evaporation rate M using Equation (3):

$$\mathrm{Q_{Evap}} = LM \quad \text{(Equation 3)}$$

where L is the specific latent heat of water. The convective heat transfer coefficient h was estimated using a simplified formula:

$$h = \frac{C\,k_{air}}{W}\left(\frac{\rho^2 g \beta C_p \Delta T \mathrm{W}^3}{\mu^2} \cdot \frac{\mu}{C_p k_{air}}\right)^n \quad \text{(Equation 4)}$$

where the constant C and n for a horizontal plate are 1.32 and 0.25, respectively; W is the width of the evaporator surface; k_{air}, ρ, β, μ and C_p are the thermal conductivity, density, thermal expansion coefficient, dynamic viscosity and heat capacity of air; and ΔT is the temperature difference between ambient air and the

evaporative surface. The numerical simulations were conducted under the steady and transient analysis mode. Temperature distribution and heat transfer flux were obtained based on the simulation results.

Life Cycle Assessment. The Janus wood evaporators from this study were compared to three other systems modeled in this paper:

1) An aerogel Janus evaporator (AJE) consisting of carbon nanotubes and cellulose nanofiber, with a similar reported evaporation rate and testing conditions (~1.2 kg/m^2 at 1 sun and 12% NaCl).[34] Note that the maximum NaCl concentration tested with the AJE was less than the concentration used in this study (20%). Therefore, it is likely that the results here undercount the actual emissions from that process.
2) An electrospun Janus mat (EJM) composed of PMMA and PAN fibers covered in carbon black nanoparticles, operating under 20% NaCl at the same conditions as the tested Janus wood.[24] Note that the EJM consisted of a thick foam and wick, which was not modeled in this analysis due to a lack of material detail provided in the initial study. Therefore, it is likely that the results here undercount the actual emissions from that process.
3) A simplified RO system powered by either photovoltaics (PV) or on-grid (OG) energy, based on Jijakli et al., modeled in this work.

Goal and Scope Definition: The objective of this study was to compare the GWP of the Janus wood evaporator to three other systems of interest, primarily from the

production phase and use phase of each system. Construction, digging, and brine and waste disposal were not in the scope of this analysis. The functional unit is 1 m^3 of highly saline solution (20 wt% NaCl) treated per day over a 20-year system lifetime, where the final goal was ZLD each day. Other assumptions, including evaporator efficacy, hours of sunlight, and specific sun power at the evaporator surface can each be found in Supplementary **Table S2**. Life-cycle impact assessment (LCA) of the designed evaporators was used to calculate GWP, while ecoinvent v3.5 and OpenLCA 10.1.3 were utilized to quantify these impacts.

Inventory Analysis: The life cycle inventory for each system included a polyvinylchloride tank, pumps to pump brine into the tank, photovoltaic cells to power the pumps, pipes, and anti-scalants and anti-foulants,[35] each of which lasted for a total of 20 years. In the LCA models, each evaporator was used 100, 1000, or 7300 times (days), under the assumption that each would eventually become saturated by salt deposits, lose efficacy, and need to be replaced by a virgin evaporator. The inventories for each evaporator, including assumptions and calculation derivations are included in the *Supporting Information* (Supplementary Table **S5-S8**). Note that most LCA data related to individual unit processes was taken from the ecoinvent 3.5 database, unless otherwise stated.

Impact Assessment: The environmental impact of each evaporator system was determined using the 20a IPCC 2013 method, which measure the 20-year greenhouse

gas emissions (CO_2 equivalent, CO_{2e}) per functional unit. This approach was also used for each of the use phase conditions (100 uses, 1000 uses, 7300 uses).

Acknowledgement

The authors thank the support from Princeton Catalysis Initiative (PCI) and the Andlinger Center for Energy and the Environment at Princeton University. We acknowledge the use of Princeton's Imaging and Analysis Center, which is partially supported through the Princeton Center for Complex Materials (PCCM), a National Science Foundation (NSF)-MRSEC program (DMR-2011750), a National Science Foundation (NSF) Materials Research Science and Engineering Center (MRSEC; DMR-1420541).

References

1. WWAP, (United Nations World Water Assessment Programme). The United Nations world water development report 2019_ leaving no one behind - UNESCO Digital Library.pdf. *Leaving no one behind* (2019).
2. Werber, J. R., Osuji, C. O. & Elimelech, M. Materials for next-generation desalination and water purification membranes. *Nature Reviews Materials* (2016) doi:10.1038/natrevmats.2016.18.
3. Koros, W. J. & Zhang, C. Materials for next-generation molecularly selective synthetic membranes. *Nat. Mater.* (2017) doi:10.1038/nmat4805.
4. Jones, E., Qadir, M., van Vliet, M. T. H., Smakhtin, V. & Kang, S. mu. The state of desalination and brine production: A global outlook. *Science of the Total Environment* (2019) doi:10.1016/j.scitotenv.2018.12.076.
5. Lee, K. P., Arnot, T. C. & Mattia, D. A review of reverse osmosis membrane materials for desalination-Development to date and future potential. *Journal of Membrane Science* (2011) doi:10.1016/j.memsci.2010.12.036.
6. Tong, T. & Elimelech, M. The Global Rise of Zero Liquid Discharge for Wastewater Management: Drivers, Technologies, and Future Directions. *Environmental Science and Technology* (2016) doi:10.1021/acs.est.6b01000.
7. Davenport, D. M., Deshmukh, A., Werber, J. R. & Elimelech, M. High-Pressure Reverse Osmosis for Energy-Efficient Hypersaline Brine Desalination: Current Status, Design Considerations, and Research Needs. *Environ. Sci. Technol. Lett.* (2018) doi:10.1021/acs.estlett.8b00274.

8. Zhao, F., Guo, Y., Zhou, X., Shi, W. & Yu, G. Materials for solar-powered water evaporation. *Nature Reviews Materials* (2020) doi:10.1038/s41578-020-0182-4.

9. Finnerty, C., Zhang, L., Sedlak, D. L., Nelson, K. L. & Mi, B. Synthetic Graphene Oxide Leaf for Solar Desalination with Zero Liquid Discharge. *Environ. Sci. Technol.* (2017) doi:10.1021/acs.est.7b03040.

10. Zhang, C. *et al.* Designing a next generation solar crystallizer for real seawater brine treatment with zero liquid discharge. *Nature Communications* **12**, 998 (2021). doi:10.1038/s41467-021-21124-4.

11. Tao, P. *et al.* Solar-driven interfacial evaporation. *Nature Energy* (2018) doi:10.1038/s41560-018-0260-7.

12. Ni, G. *et al.* A salt-rejecting floating solar still for low-cost desalination. *Energy Environ. Sci.* (2018) doi:10.1039/c8ee00220g.

13. He, S. *et al.* Nature-inspired salt resistant bimodal porous solar evaporator for efficient and stable water desalination. *Energy Environ. Sci.* **12**, 1558–1567 (2019).

14. Li, X. *et al.* Graphene oxide-based efficient and scalable solar desalination under one sun with a confined 2D water path. *Proc. Natl. Acad. Sci. U. S. A.* (2016) doi:10.1073/pnas.1613031113.

15. Li, R., Zhang, L., Shi, L. & Wang, P. MXene Ti3C2: An Effective 2D Light-to-Heat Conversion Material. *ACS Nano* (2017) doi:10.1021/acsnano.6b08415.

16. Zhao, F. *et al.* Highly efficient solar vapour generation via hierarchically nanostructured gels. *Nat. Nanotechnol.* (2018) doi:10.1038/s41565-018-0097-z.

17. Ni, G. *et al.* Steam generation under one sun enabled by a floating structure with thermal concentration. *Nat. Energy* (2016) doi:10.1038/nenergy.2016.126.

18. Shi, Y. *et al.* A 3D Photothermal Structure toward Improved Energy Efficiency in Solar Steam Generation. *Joule* (2018) doi:10.1016/j.joule.2018.03.013.

19. Cao, S. *et al.* Advances in solar evaporator materials for freshwater generation. *J. Mater. Chem. A* (2019) doi:10.1039/c9ta06034k.

20. Wu, L. *et al.* Highly efficient three-dimensional solar evaporator for high salinity desalination by localized crystallization. *Nat. Commun.* (2020) doi:10.1038/s41467-020-14366-1.

21. Pang, Y. *et al.* Solar–Thermal Water Evaporation: A Review. *ACS Energy Lett.* (2020) doi:10.1021/acsenergylett.9b02611.

22. Cooper, T. A. *et al.* Contactless steam generation and superheating under one sun illumination. *Nat. Commun.* (2018) doi:10.1038/s41467-018-07494-2.

23. Xia, Y. *et al.* Spatially isolating salt crystallisation from water evaporation for continuous solar steam generation and salt harvesting. *Energy Environ. Sci.* (2019) doi:10.1039/c9ee00692c.

24. Xu, W. *et al.* Flexible and Salt Resistant Janus Absorbers by Electrospinning for Stable and Efficient Solar Desalination. *Adv. Energy Mater.* (2018) doi:10.1002/aenm.201702884.

25. Yang, Y. *et al.* A Two-Dimensional Flexible Bilayer Janus Membrane for Advanced Photothermal Water Desalination. *ACS Energy Lett.* (2018) doi:10.1021/acsenergylett.8b00433.

26. Dudchenko, A. V., Chen, C., Cardenas, A., Rolf, J. & Jassby, D. Frequency-dependent stability of CNT Joule heaters in ionizable media and desalination processes. *Nat. Nanotechnol.* (2017) doi:10.1038/nnano.2017.102.

27. Panagopoulos, A., Haralambous, K. J. & Loizidou, M. Desalination brine disposal methods and treatment technologies - A review. *Science of the Total Environment* (2019) doi:10.1016/j.scitotenv.2019.07.351.

28. Kuang, Y. *et al.* A High-Performance Self-Regenerating Solar Evaporator for Continuous Water Desalination. *Adv. Mater.* (2019) doi:10.1002/adma.201900498.

29. Zhao, J. *et al.* A hydrophobic surface enabled salt-blocking 2D Ti3C2 MXene membrane for efficient and stable solar desalination. *J. Mater. Chem. A* (2018) doi:10.1039/c8ta05569f.

30. Chen, X., Zhu, X., He, S., Hu, L. & Ren, Z. J. Advanced Nanowood Materials for the Water–Energy Nexus. *Adv. Mater.* (2020) doi:10.1002/adma.202001240.

31. Hou, D. *et al.* Hydrophobic nanostructured wood membrane for thermally efficient distillation. *Sci. Adv.* **5**, eaaw3203 (2019).

32. Menon, A. K., Haechler, I., Kaur, S., Lubner, S. & Prasher, R. S. Enhanced solar evaporation using a photo-thermal umbrella for wastewater management. *Nat. Sustain.* (2020) doi:10.1038/s41893-019-0445-5.

33. Arvanitoyannis, I. S. ISO 14040: Life Cycle Assessment (LCA) - Principles and Guidelines. in *Waste Management for the Food Industries* (2008). doi:10.1016/B978-012373654-3.50006-7.

34. Hu, R. *et al.* A Janus evaporator with low tortuosity for long-term solar desalination. *J. Mater. Chem. A* (2019) doi:10.1039/c9ta01576k.

35. Jijakli, K., Arafat, H., Kennedy, S., Mande, P. & Theeyattuparampil, V. V. How green solar desalination really is? Environmental assessment using life-cycle analysis (LCA) approach. *Desalination* (2012) doi:10.1016/j.desal.2011.09.038.

36. Lu, L. *et al.* Unbiased solar H<inf>2</inf> production with current density up to 23 mA cm^{-2} by Swiss-cheese black Si coupled with wastewater bioanode. *Energy Environ. Sci.* **12**, (2019).

Figures

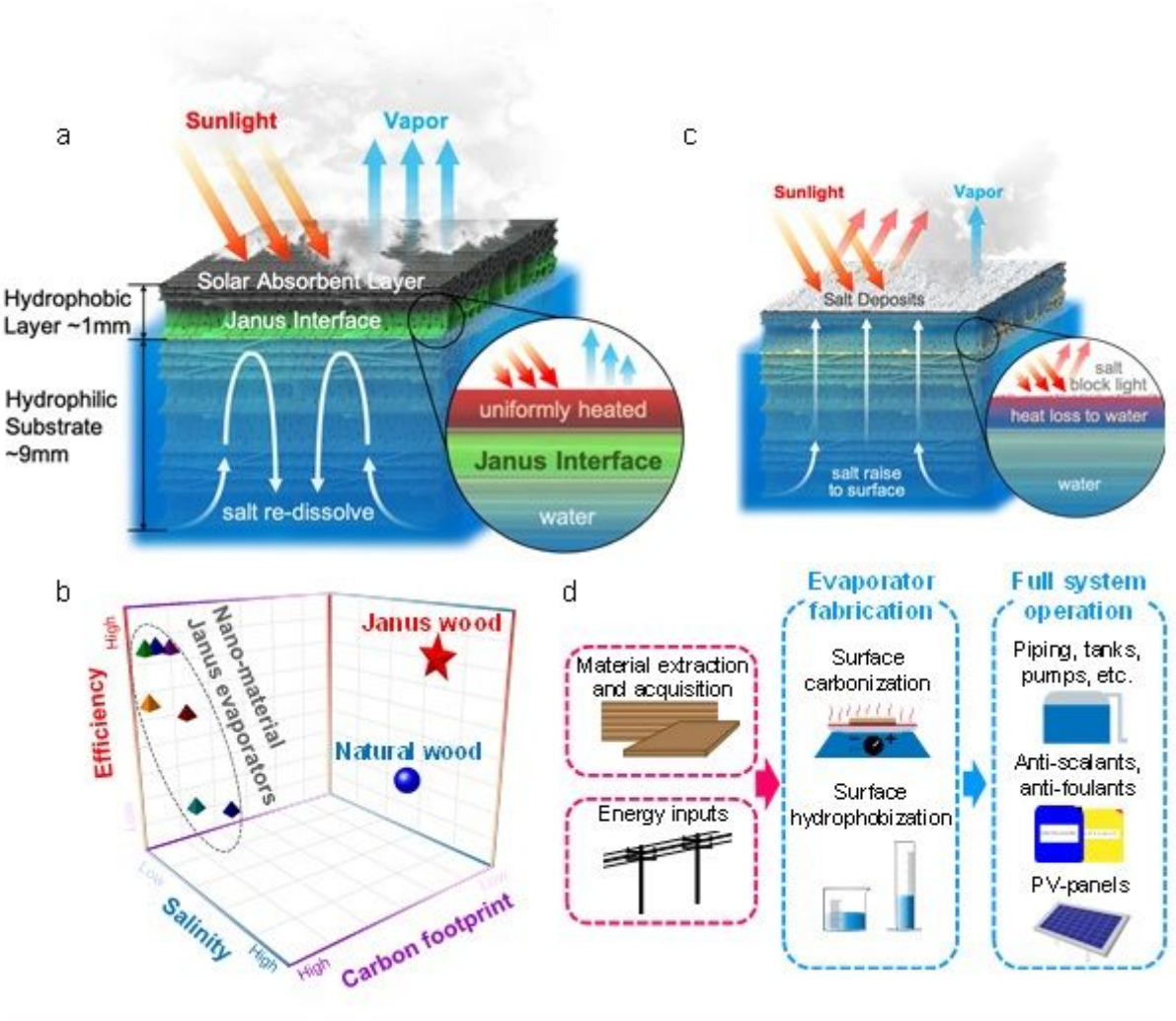

Figure 1

Janus wood as a salt-resistant and sustainable evaporator. a, Schematic of the Janus wood evaporator for solar distillation, where the Janus interface enhanced thermal insulation and improved performance. b, Performance comparison of Janus wood evaporator, natural wood evaporator and nanomaterial-based Janus thin-film evaporator. c, Salt accumulation caused severe performance decay in a natural wood evaporator. d, Scope of the life cycle assessment for the Janus wood evaporator ZLD system.

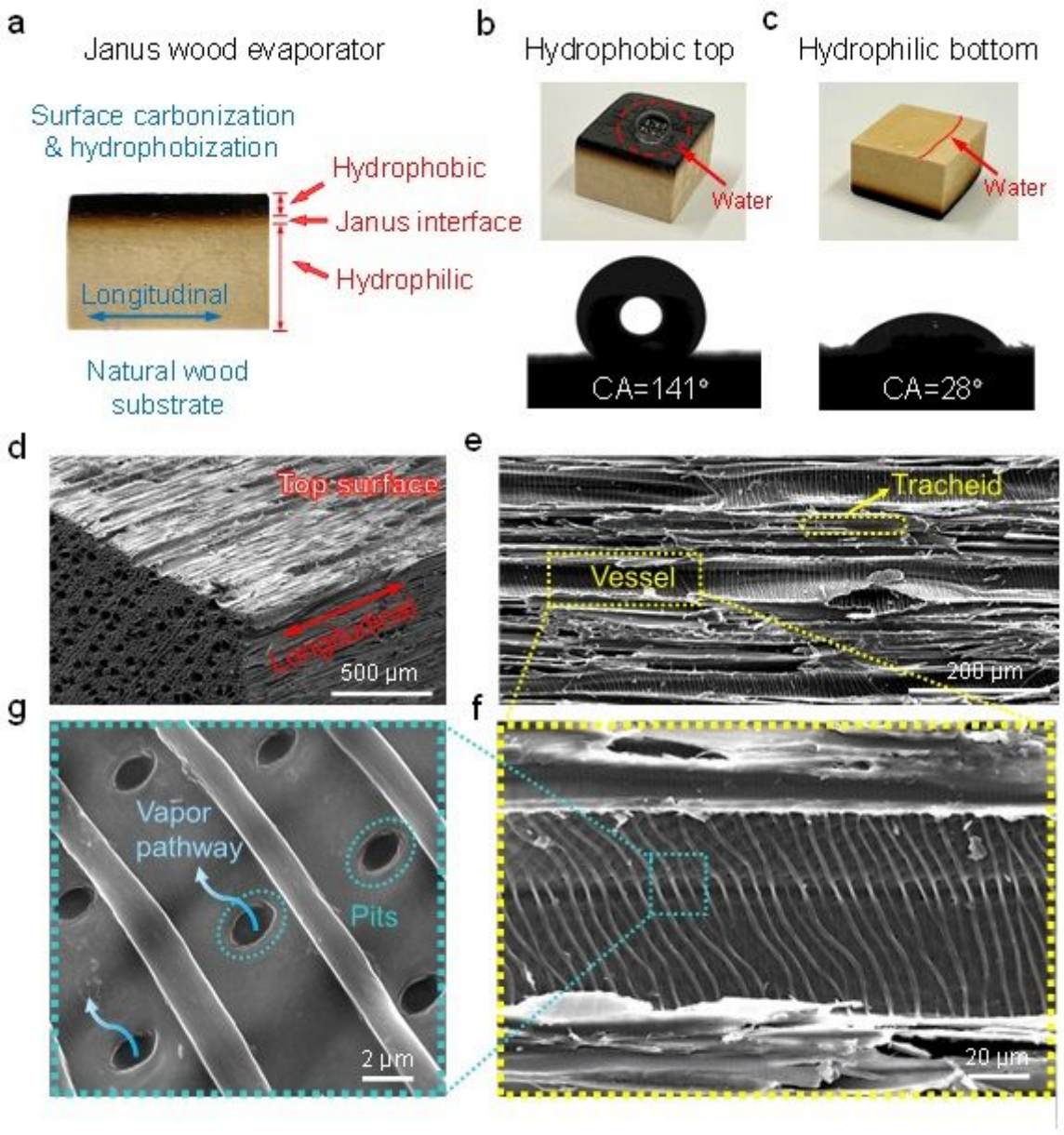

Figure 2

Characterization showing the asymmetric wettability and the hierarchical porous structure of the Janus wood evaporator. a, The digital image of Janus wood evaporator. b, The top surface was modified into hydrophobic with a large contact angle (CA) and rejected water penetration. c, The bottom layer maintained the hydrophilic nature of wood and was quickly wetted by water drops. d, SEM image showing the hierarchical structure of Janus wood. e, Magnified SEM image showing aligned vessels and tracheid on the top surface, f, Magnified SEM image showing vessel wall structure. g, magnified SEM images showing the abundantly distributed pits on the vessel wall.

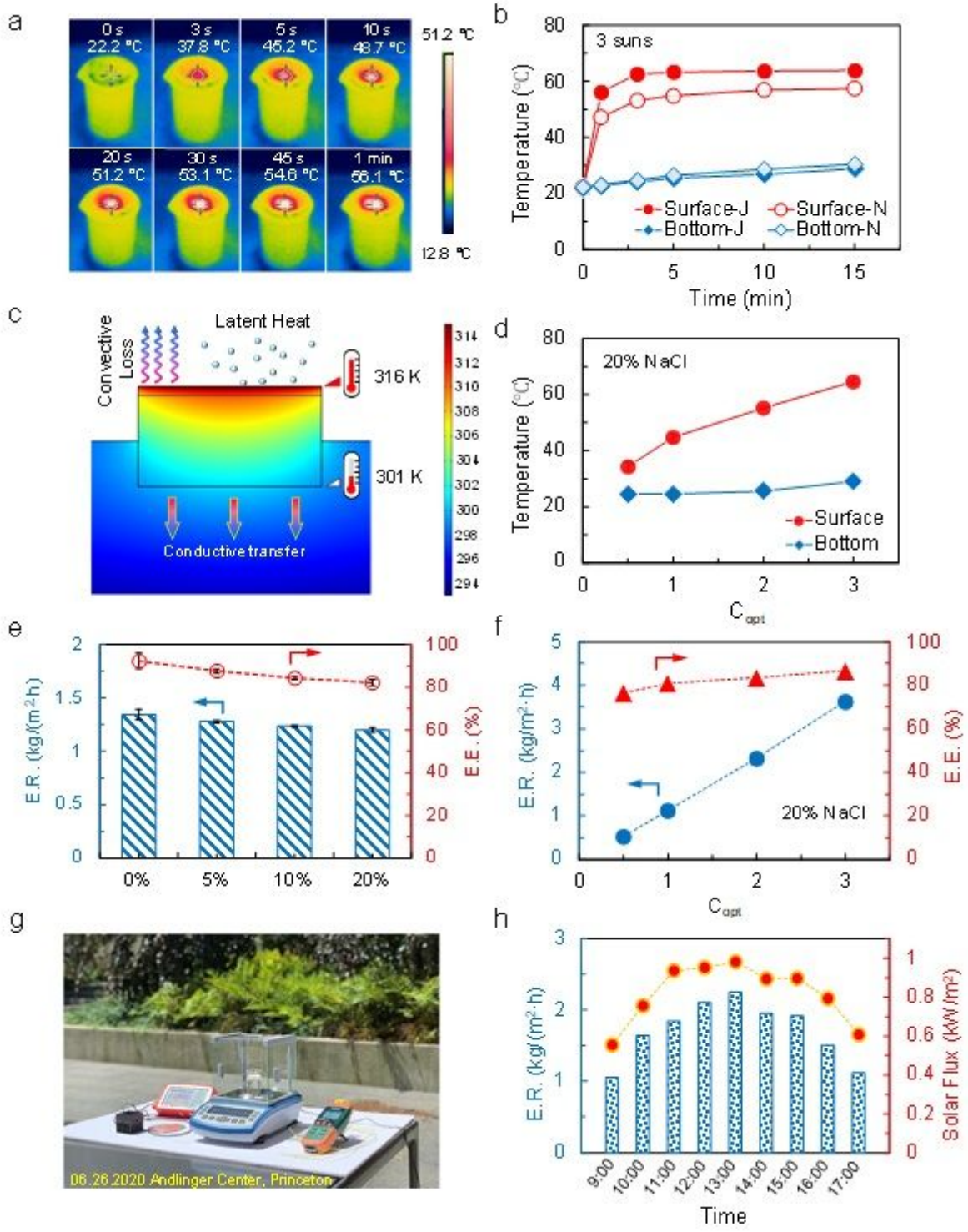

Figure 3

High solar distillation performance of Janus wood evaporator in lab conditions and field tests. a, IR images of the solar distillation module under 3 suns at increasing times up to 60s. b, Time-dependent surface temperature changes of the Janus wood (J) and natural wood control (N) under 3 suns illumination. c, Cross-sectional temperature profile of the Janus wood evaporator and the bulk brine under 1 sun incident, modelled with COMSOL, indicating the hydrophobic top layer improved heat insulation and localization. d, Surface temperature changes of Janus wood under different optical concentrations.

e, The evaporation rate (E.R.) and evaporation efficiency (E.E.) of Janus wood under different salinities. f, The E.R. and E.E. of Janus wood under different solar incident concentrations. g, Digital image of the solar distillation module setup. h, The hourly-average E.R. corresponding to the hourly-average natural solar flux.

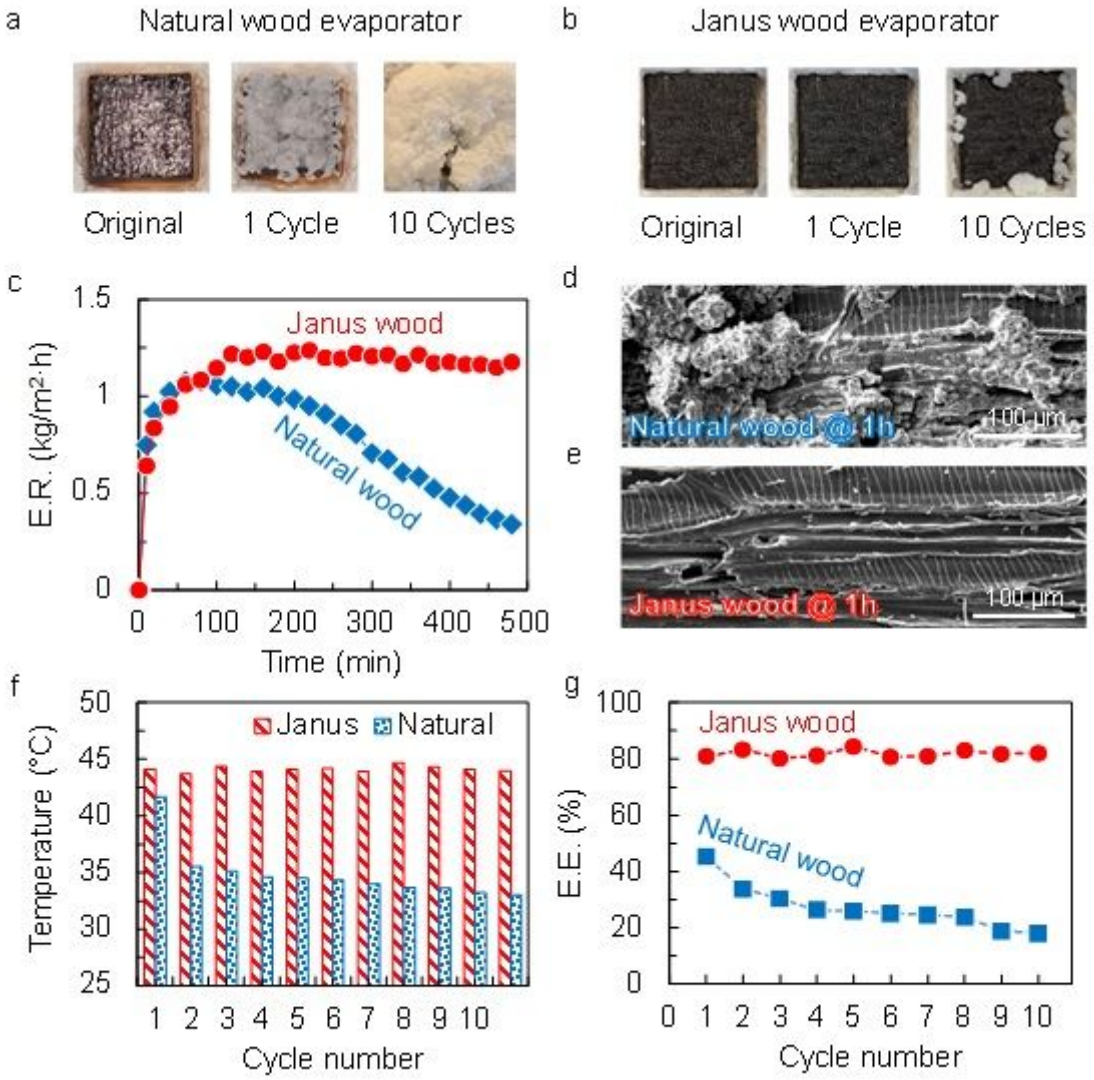

Figure 4

Longevity tests of the Janus wood and natural wood. a, Digital images of the natural wood evaporator before cycling experiments, after the 1st cycle, and after the 10th cycle. b, Digital images of the Janus wood evaporator before cycling experiments, after the 1st cycle, and after the 10th cycle. c, The evaporation rate (E.R.) of the wood evaporators during the 1st cycle. d, SEM image of the top surface of the natural wood evaporator after operating for 1 hour in the 1st cycle. e, SEM image of the top surface of the Janus wood after operating for 1 hour in the 1st cycle. f, The surface temperature of the Janus wood v.s. natural wood in each of the 10 cycles. g, The evaporation efficiency (E.E.) of the Janus wood and natural wood in each of the 10 cycles.

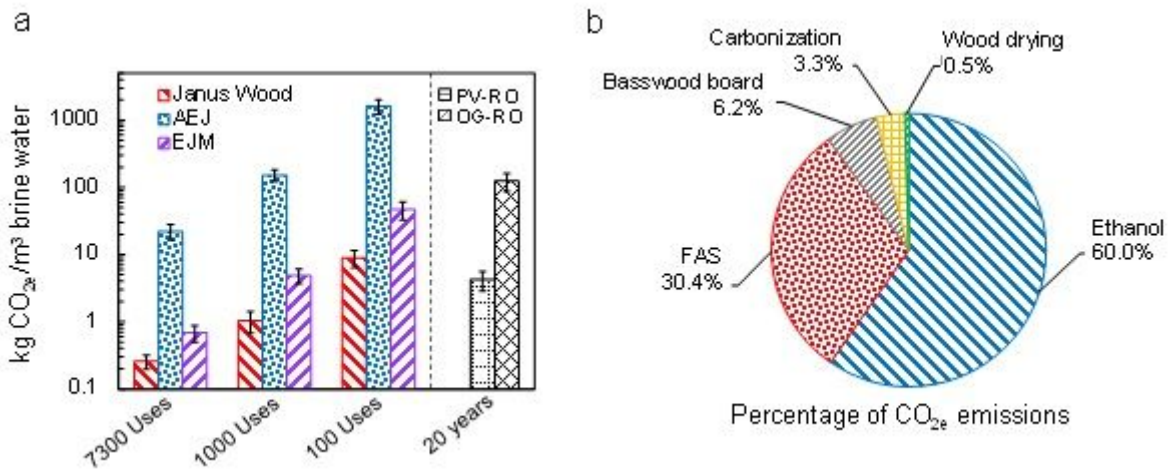

Figure 5

Preliminary LCA of the Janus wood evaporator and three other systems. a, The global warming potential of Janus wood evaporator, aerogel Janus evaporator (AEJ), and electrospun Janus mat (EJM), as it relates to the lifetime of each evaporator, as well as the global warming potential of photovoltaic (PV) and on-grid (OG) electricity-powered reverse osmosis (RO) systems. b, The relative CO2e emissions of each process or material involved in the production of Janus wood evaporators.

Supplementary Files

This is a list of supplementary files associated with this preprint. Click to download.

- JanuswoodEvaporatorSI2.16.2020.docx